Acta Crystallographica Section B
Structural Science
ISSN 0108-7681

Influence of the molecular structures on the high-pressure and low-temperature phase transitions of plastic crystals

Markus Wunschel,[a] Robert E. Dinnebier,[a,b] Stefan Carlson,[c]† Piotr Bernatowicz[d] and Sander van Smaalen[a]*

[a]Laboratory of Crystallography, University of Bayreuth, D-95440 Bayreuth, Germany, [b]Max-Planck Institute for Solid State Research, Heisenbergstrasse 1, D-70569 Stuttgart, Germany, [c]High Pressure Group, ESRF, BP 220, F-38043 Grenoble CEDEX, France, and [d]Institute of Organic Chemistry, Polish Academy of Sciences, PO Box 8, PL-01-224 Warsaw 42, Poland

† Current address: Inorganic Chemistry, Lund University, PO Box 124, SE-22100 Lund, Sweden

Correspondence e-mail: smash@uni-bayreuth.de

Received 22 August 2002
Accepted 18 November 2002

The crystal structures of *tert*-butyl-tris(trimethylsilyl)silane, $Si[C(CH_3)_3]_1[Si(CH_3)_3]_3$ (Bu1), and di-*tert*-butyl-bis(trimethylsilyl)silane, $Si[C(CH_3)_3]_2[Si(CH_3)_3]_2$ (Bu2), at room temperature and at 105 K have been determined by X-ray powder diffraction; the high-pressure behavior for pressures between 0 and 5 GPa is reported. The room-temperature structures have cubic $Fm\bar{3}m$ symmetry ($Z = 4$) with $a = 13.2645$ (2) Å, $V = 2333.87$ (4) Å^3 for Bu1 and $a = 12.9673$ (1) Å, $V = 2180.46$ (3) Å^3 for Bu2. The molecules are arranged in a cubic close packing (c.c.p.) and exhibit at least 48-fold orientational disorder. Upon cooling both compounds undergo a first-order phase transition at temperatures $T_c = 230$ (5) K (Bu1) and $T_c = 250$ (5) K (Bu2) into monoclinic structures with space group $P2_1/n$. The structures at 105 K have $a = 17.317$ (1), $b = 15.598$ (1), $c = 16.385$ (1) Å, $\gamma = 109.477$ (4)°, $V = 4172.7$ (8) Å^3 and $Z = 8$ for Bu1 and $a = 17.0089$ (9), $b = 15.3159$ (8), $c = 15.9325$ (8) Å, $\gamma = 110.343$ (3)°, $V = 3891.7$ (5) Å^3 and $Z = 8$ for Bu2. The severe disorder of the room-temperature phase is significantly decreased and only a two- or threefold rotational disorder of the molecules remains at 105 K. First-order phase transitions have been observed at pressures of 0.13–0.28 GPa for Bu1 and 0.20–0.24 GPa for Bu2. The high-pressure structures are isostructural to the low-temperature structures. The pressure dependencies of the unit-cell volumes were fitted with Vinet equations of state and the bulk moduli were obtained. At still higher pressures further anomalies in the pressure dependencies of the lattice parameters were observed. These anomalies are explained as additional disorder–order phase transitions.

1. Introduction

tert-Butyl-tris(trimethylsilyl)silane, $Si[C(CH_3)_3]_1[Si(CH_3)_3]_3$ (hereafter denoted by Bu1), and di-*tert*-butyl-bis(trimethylsilyl)silane, $Si[C(CH_3)_3]_2[Si(CH_3)_3]_2$ (hereafter denoted by Bu2), belong to the class of plastic crystals, *i.e.* crystalline compounds with freely rotating molecules on well defined sites. Unlike the molecules $Si[Si(CH_3)_3]_4$ or $C[Si(CH_3)_3]_4$, which are almost spherically shaped, Bu1 and Bu2 can be approximately described as spheres with dents (Figs. 1 and 2). In $Si[Si(CH_3)_3]_4$ four $Si(CH_3)_3$ groups are bonded to the central Si atom, and the four non-central Si atoms form a regular 'core' tetrahedron. Bu1 and Bu2 are obtained by replacing one (Bu1) or two (Bu2) of the $Si(CH_3)_3$ groups with $C(CH_3)_3$ groups. This change leads to deformed core tetrahedra formed from three Si atoms and one C atom in Bu1 and two Si atoms and two C atoms in Bu2. The consequences for the molecular symmetry are that Bu1 may only have C_{3v} symmetry while Bu2 may only have C_{2v} symmetry.

© 2003 International Union of Crystallography
Printed in Great Britain – all rights reserved

The rotator phases of compounds $E[X(CH_3)_3]_4$, with E = C, Si, Ge and X = C, Si, Sn, are isostructural. The rotating molecules form a cubic-close-packed (c.c.p.) arrangement with space group $Fm\bar{3}m$ and lattice parameters between a = 12.8902 $\{C[Si(CH_3)_3]_4\}$ and a = 14.2037 Å $\{Ge[Sn(CH_3)_3]_4\}$ (Dinnebier *et al.*, 1999, 2002). On cooling, transitions occur towards ordered or partially ordered phases. It has been found that both the transition temperatures and the nature of the ordered phases are different for the different compounds. $C[Si(CH_3)_3]_4$ and $Si[Si(CH_3)_3]_4$ remain cubic in their low-temperature phases, but the reduced symmetry allows for a complete ordering of the molecules (space group $P2_13$). In the case of $Si[Si(CH_3)_3]_4$ there is a single transition, but for $C[Si(CH_3)_3]_4$ an intermediate phase exists with space group $Pa\bar{3}$ (Dinnebier *et al.*, 1999). $Si[Sn(CH_3)_3]_4$ and $Ge[Sn(CH_3)_3]_4$ have triclinic low-temperature structures (space group $P\bar{1}$), which correspond to a distorted c.c.p. arrangement of the molecules. High-pressure studies have been performed for $C[Si(CH_3)_3]_4$ and $Si[Si(CH_3)_3]_4$ only. For $C[Si(CH_3)_3]_4$ two transitions were observed below a pressure of p = 4.8 GPa; these transitions resulted in phases isostructural to the low-temperature phases (Dinnebier *et al.*, 2000). For $Si[Si(CH_3)_3]_4$ two monoclinic phases were found below p = 8.7 GPa (Wunschel *et al.*, 2003).

The dynamical nature of the disorder in the plastic phases of the various compounds was confirmed by NMR (Helluy *et al.*, 1998; Dinnebier *et al.*, 2002). However, the behaviors of the molecules in the ordered phases were found to differ widely. The multiple-peak structure of the ^{13}C resonances in $Si[Sn(CH_3)_3]_4$ and $Ge[Sn(CH_3)_3]_4$ showed that these molecules are truly static at low temperatures (Dinnebier *et al.*, 2002). However, $C[Si(CH_3)_3]_4$ and $Si[Si(CH_3)_3]_4$ exhibit reorientational jumps between the 12 equivalent orientations even in the ordered phases.

In this work we present the results of a crystallographic study of the phase transitions of Bu1 and Bu2 as a function of temperature and pressure. Using X-ray powder diffraction and Rietveld refinements we show that the room-temperature phases are again rotator phases with a c.c.p. arrangement of the molecules. A single low-temperature phase with monoclinic symmetry is found for each compound. An analysis of the crystal structures shows that the different low-temperature structures of the compounds $E[X(CH_3)_3]_{4-n}[X'(CH_3)_3]_n$ (n = 0,1,2) can be explained by the requirements of an optimal packing given the different shapes of the molecules. The application of pressure results in monoclinic structures similar to the low-temperature structures. However, at still higher pressures additional transitions are observed that are tentatively interpreted as being due to a further ordering of the molecules.

2. Experimental

$Si[C(CH_3)_3]_2[Si(CH_3)_3]_2$ has been prepared following the procedure described by Becker *et al.* (1985). $Si[C(CH_3)_3][Si(CH_3)_3]_3$ was prepared in a similar way, by replacing the reagent $[(CH_3)_3C]_2SiCl_2$, which is used for the preparation of $Si[C(CH_3)_3]_2[Si(CH_3)_3]_2$, by $[(CH_3)_3C]SiCl_3$.

2.1. High-resolution X-ray powder diffraction

2.1.1. Data collection and data reduction. X-ray powder diffraction experiments at ambient pressure in the temperature range 105–295 K were performed at the high-resolution X-ray powder diffractometer at beamline BM16 of the European Synchrotron Radiation Facility (ESRF) (Table 1). A wavelength of 0.399828 (2) Å was selected with an Si(111) double monochromator. Slits were used to adjust the size of the beam to 2 × 0.6 mm^2. The samples were loaded into 0.5 mm lithium borate glass (glass No. 50) capillaries, which were spun during the measurements to improve randomiza-

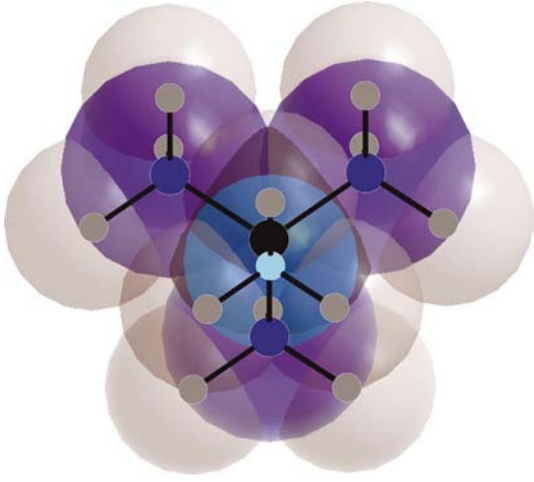

Figure 1
An $Si[C(CH_3)_3]_1[Si(CH_3)_3]_3$ (Bu1) molecule. The central Si atom (black) is surrounded by three Si atoms and one C atom, which are terminated by three methyl groups each (C of methyl groups: light gray). The H atoms of the methyl groups are not shown. The space-filling model represents van der Waals' radii. The picture was generated by *DIAMOND* software.

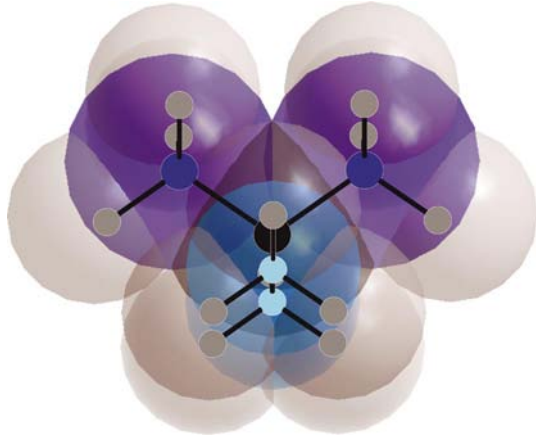

Figure 2
An $Si[C(CH_3)_3]_2[Si(CH_3)_3]_2$ (Bu2) molecule. The central Si atom (black) is surrounded by two Si atoms and two C atoms, which are terminated by three methyl groups each (C of methyl groups: light gray). The H atoms of the methyl groups are not shown. The space-filling model represents van der Waals' radii. The picture was generated by *DIAMOND* software.

Table 1
Experimental table.

	Bu1		Bu2	
Chemical formula	$Si[C(CH_3)_3][Si(CH_3)_3]_3$		$Si[C(CH_3)_3]_2[Si(CH_3)_3]_2$	
Chemical formula weight	304.8		288.7	
Temperature (K)	295	105	295	105
Cell setting, space group	Cubic, $Fm\bar{3}m$	Monoclinic, $P2_1/n$	Cubic, $Fm\bar{3}m$	Monoclinic, $P2_1/n$
a (Å)	13.2645 (2)	17.317 (1),	12.9673 (1)	17.0089 (9)
b (Å)		15.598 (1)		15.3159 (8)
c (Å)		16.385 (1)		15.9325 (8)
γ (°)		109.477 (4)		110.343 (3)
V (Å^3)	2333.87 (4)	4172.7 (5)	2180.46 (3)	3891.7 (5)
Z	4	8	4	8
D_x (Mg m^{-3})	0.867 (1)	0.970 (1)	0.879 (1)	0.986 (1)
μ (cm^{-1})	0.19	0.22	0.15	0.18
Radiation type	Synchrotron	Synchrotron	Synchrotron	Synchrotron
Wavelength (Å)	0.399828 (2)	0.399828 (2)	0.399828 (2)	0.399828 (2)
2θ range (°)	1.1–21.5	1.4–14.0	0.4–28.0	0.5–14.0
R_p (Le Bail)	0.193	0.043	0.136	0.050
R_{wp} (Le Bail)	0.265	0.056	0.194	0.066
R_p (Rietveld)	0.197	0.066	0.146	0.067
R_{wp} (Rietveld)	0.268	0.084	0.205	0.089
R_{Bragg}	0.047	0.048	0.14	0.043
χ^2	1.12	0.58	1.75	0.63
No. of parameters	13	60	12	74
No. of restraints	–	6	–	6
No. of reflections	73	993	137	927
with $I \geq 3\sigma(I)$	6	125	11	155
No. of data points	4081	4200	9201	4500

Computer programs: *JANA*2000 (Petříček & Dušek, 2000); *DASH* (David & Shankland, 2001).

tion of the samples. The temperature of the samples was controlled with an Oxford Cryosystems cold-nitrogen-gas blower. The diffracted intensities were collected with a nine-crystal analyzer stage (Hodeau *et al.*, 1998) [nine Ge(111) crystals separated by 2° intervals and nine Na(Tl)I scintillation counters]. The incident beam was monitored by an ion chamber to allow for normalization of the measured data by the primary-beam intensity. More details of the experimental setup are described by Fitch (1996).

The samples were cooled from room temperature to 105 K in steps of 10 K. At each temperature a fast data collection of approximately 15 min was made. Additionally, data for Bu2 at room temperature were collected in a scan running for 1 h. Data at 105 K were collected in several scans over the same angular range, so that the total measurement time was 13.5 h for Bu1 and 12.5 h for Bu2. All data were recorded in a continuous scanning mode. The data reduction included normalization against monitor counts, binning of the output of the detectors, summation of repeated scans where applicable, and conversion to step-scan data.

Indexing of the low-temperature data at 105 K was performed with the program *KOHL* (Kohlbeck & Hörl, 1976, 1978), which is part of the *CRYSFIRE* indexing suite (Shirley, 2000). All data sets up to 225 K for Bu1 and 245 K for Bu2 could be indexed with monoclinic lattices. For temperatures of 235 K and higher (Bu1) and 255 K and higher (Bu2) *F*-centered cubic lattices were found.

The lattice parameters as a function of temperature were determined by Le Bail-type fits (Le Bail *et al.*, 1988) of the data, which employed the computer programs *JANA*2000 (Petříček & Dušek, 2000; Dušek *et al.*, 2001) and *GSAS* (Larson & von Dreele, 1994). The asymmetric peak profiles were described with a pseudo-Voigt profile function (Thompson *et al.*, 1987) and correction for asymmetry due to axial divergence (Finger *et al.*, 1994). A combination of a manual background, which was determined with the program *GUFI* (Dinnebier & Finger, 1998), and a Legendre polynomial with four or five terms (*JANA*2000), or a cosine Fourier series with four terms (*GSAS*), was used. Lattice parameters for the various temperatures are available as supplementary material.[1]

The X-ray diffraction patterns thus showed the presence of phase transitions at T_c = 230 (5) K for Bu1 and at T_c = 250 (5) K for Bu2 (Figs. 3 and 4). An analysis of extinction conditions in the data taken at the lowest temperatures gave the space group $P2_1/n$. The distinction between $P2_1/n$ and $P2_1/a$ could be made on the basis of two peaks at $2\Theta = 4.495°$ and $2\Theta = 5.450°$ in the pattern of Bu2, because these peaks were not indexed in the latter setting. The validity of the space group was confirmed by Rietveld refinement.

2.1.2. Refinement of Bu1 at 105 K. The starting points for the Rietveld refinements of the structure at 105 K were the background and profile functions as determined by the Le Bail fit. An initial structure model for Bu1 was obtained by global optimization techniques (David *et al.*, 1998) with the program *DASH*[2] (David & Shankland, 2001). Other structures that have been successfully solved from powder data using *DASH*

[1] Supplementary data for this paper are available from the IUCr electronic archives (Reference: OS0101). Services for accessing these data are described at the back of the journal.
[2] *DASH* is a product of the Cambridge Crystallographic Data Centre, 12 Union Road, Cambridge CB2 1EZ, England.

include tetracine hydrochloride (Nowell *et al.*, 2002) and decafluoroquarterphenyl (Smrcok *et al.*, 2001). Molecular crystals at high pressures have been studied with X-ray powder diffraction by *e.g.* Fujiki *et al.* (2002) and Nakayama *et al.* (2000).

The unit cell of Bu1 contains two independent molecules at general positions, and these molecules contain 34 independent atoms. Refinement of the 102 independent positional parameters was not possible, so bonding distances and angles were restrained to typical values taken from the literature (*International Tables for Crystallography*, 1995, Vol. C). This refinement converged at $R_p = 0.078$, $R_{wp} = 0.098$ and $R_{Bragg} = 0.062$.

Despite the reasonably good fit, the initial model suffered from several deficiencies. Because of the restraints a true refinement of the bonding distances has not been possible. In addition, orientational disorder of the molecules was not accounted for, whereby in each direction both $C(CH_3)_3$ and $Si(CH_3)_3$ occur with fractional occupancies. To enable these extensions of the model, we have introduced quasi-rigid bodies for the molecules. All molecules are constructed from a central Si atom, one $C(CH_3)_3$ group and one $Si(CH_3)_3$ group. Each group $Si-C(CH_3)_3$ and $Si-Si(CH_3)_3$ (including the central Si atom) is defined as a group of atoms with internal threefold symmetry (Fig. 5, Table 2). The central Si atom Si(0) is placed at the origin of a Cartesian coordinate system. The second atom, Si(1) or C(1), is placed on the z axis. Finally a methyl group [C(21) or C(22)] is placed in the xz plane. The remaining two methyl groups are generated by the threefold axis parallel to the z axis. The starting values for the bond distances were taken from the literature (*International Tables for Crystallography*, 1995, Vol. C), and the Si(0)—Si(1)—C(21) and Si(0)—C(1)—C(22) angles were given the value of the tetrahedral angle of 109.47°. The H atoms of the methyl groups were not explicitly included, because the methyl groups are believed to be rotating about the Si(1)—C(21) and C(1)—C(22) bonds. The occupancies of the C atoms C(21) and C(22) were set to 1.3 to account for the contribution of the H atoms to the scattering. This occupancy could not be refined,

Table 2
Internal parameters of the quasi-rigid rotator groups from the best fit of the low-temperature structures of Bu1 and Bu2 at 105 K.

	x	y	z	U_{iso}	Occupancy
Bu1					
Rigid Body 'TMSi'					
Si(0)	0	0	0	0.073 (7)	1/4
Si(1)	0	0	0.1440 (3)	0.037 (4)	1
C(21)	0.1054 (5)	0	0.1829 (4)	0.041 (6)	1.3
Rigid Body 'TMC'					
Si(0)	0	0	0	0.073 (7)	1/4
C(1)	0	0	0.1133 (6)	0.037 (4)	1
C(22)	0.0888 (8)	0	0.1456 (7)	0.041 (6)	1.3
Bu2					
Rigid Body 'TMSi'					
Si(0)	0	0	0	0.061 (5)	1/4
Si(1)	0	0	0.1491 (4)	0.064 (5)	1
C(21)	0.1088 (5)	0	0.1908 (5)	0.019 (4)	1.3
Rigid Body 'TMC'					
Si(0)	0	0	0	0.061 (5)	1/4
C(1)	0	0	0.1239 (5)	0.064 (5)	1
C(22)	0.0942 (5)	0	0.1622 (5)	0.019 (4)	1.3

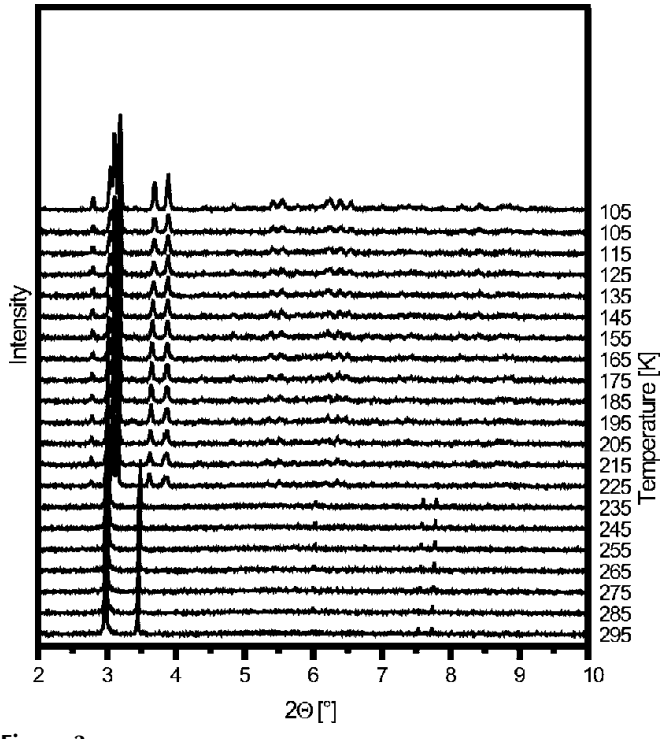

Figure 3
X-ray diffraction diagrams of the low-temperature experiments for Bu1. Note the phase transition between 235 and 225 K.

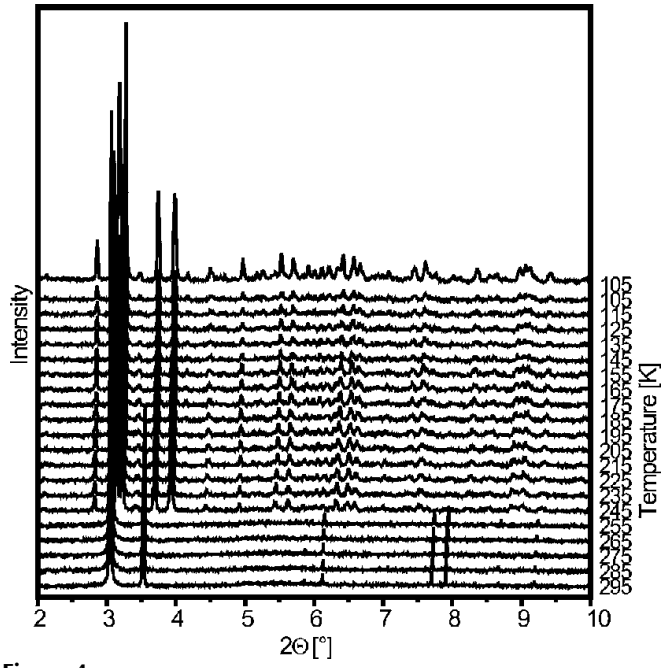

Figure 4
X-ray diffraction diagrams of the low-temperature experiments for Bu2. Note the phase transition between 255 and 245 K.

because it is correlated with the (refined) temperature factor. For each group, three internal degrees of freedom remained; these were taken as the z coordinate of Si(1) or C(1) and the x and z coordinates of C(21) and C(22).

One molecule of Bu1 can be constructed from one group of $Si-C(CH_3)_3$ and three copies of the $Si-Si(CH_3)_3$ group with their central atoms Si(0) coinciding at the center of the molecule and with the Si(0)—Si(1) and Si(0)—C(1) bonds pointing in the appropriate directions. A set of four molecules disordered over one site is obtained with four copies of both groups; these copies are placed with their Si(0)—Si(1) and Si(0)—C(1) bonds coinciding pairwise. The sum of occupancies in each direction was restricted to 1.0, the sum of occupancies of $Si-C(CH_3)_3$ was set to 1.0, and the sum of occupancies of $Si-Si(CH_3)_3$ was restricted to 3.0. Thus three parameters that describe the orientational disorder remained in the refinement. The directions of the $Si-C(CH_3)_3$ and $Si-Si(CH_3)_3$ groups were described by the Eulerian angles φ and χ as defined in *JANA*2000. The starting values were taken from the initial refinement. Constraints were applied on the directions of the Si(0)—Si(1) and the Si(0)—C(1) bonds by enforcing identical φ and χ angles for both rotator groups. The rotations of the methyl groups about the Si(0)—Si(1) and Si(0)—C(1) axes, which were described by the Eulerian angles ψ, were refined independently (Table 3). During the refinements the $Si-C(CH_3)_3$ occupancies of two directions of the first molecular site and of one direction of the second molecular site became equal to 0 and were afterwards fixed at this value. For these cases the corresponding ψ angles were also fixed. In the remaining directions, the $Si-Si-(CH_3)_3$ and $Si-C-(CH_3)_3$ occupancies are finite. It became apparent that for the first site the distribution of $Si-C(CH_3)_3$ in the two remaining directions is almost identical, while for the second site one of the three directions is favored (Table 3). Three isotropic temperature factors were refined: one for Si(0), one for Si(1) and C(1), and one for C(21) and C(22).

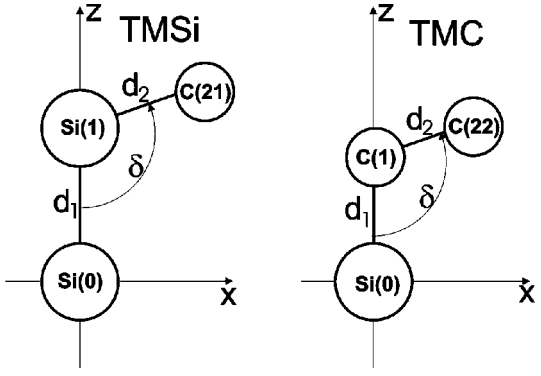

Figure 5
Definition of the quasi-rigid bodies used to describe the Bu1 and Bu2 molecules in the Rietveld refinements at 105 K. The values of the distance restraints d_1 = 1.887 (10) Å and d_2 = 1.534 (20) Å for $Si-C-(CH_3)_3$ and d_1 = 2.359 (10) Å and d_2 = 1.857 (20) Å for $Si-C-(CH_3)_3$ were taken from the literature. The angle δ was restrained to the tetrahedral angle of 109.45 (25)°.

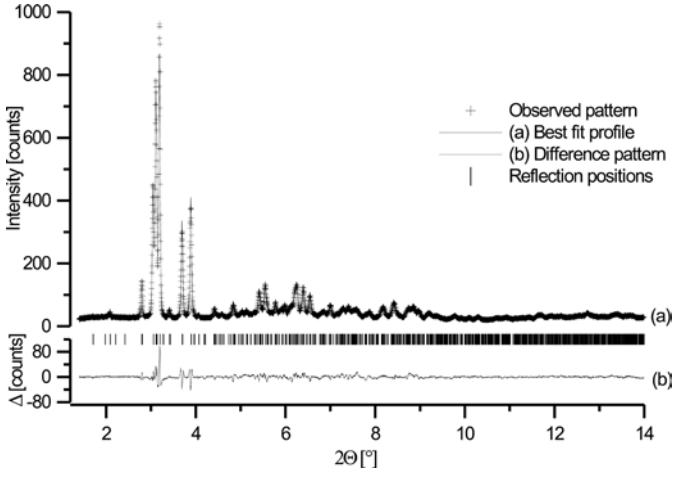

Figure 6
Best fit profile of the Rietveld refinement of Bu1 at 105 K with disordered rigid rotator groups.

Table 3
Orientation of the quasi-rigid rotator groups TMC and TMSi are defined in Table 2.

The groups with sequence numbers 1–4 are used to describe the first molecule with the center at [0.1553 (7), 0.2422 (9), 0.38867 (8)] (Bu1) and [0.1469 (8), 0.2438 (8), 0.3627 (7)] (Bu2). Groups with sequence numbers 5–8 describe the second molecule with the center at [0.3431 (9), 0.771 (1), 0.6135 (9)] (Bu1) and [0.3413 (7), 0.7739 (7), 0.6184 (7)] (Bu2).

	Occupancy	φ	χ	ψ
Bu1				
First molecule				
TMC#1	0.51 (2)	−126.9 (9)	39.7 (5)	170.0 (3)
TMC#4	0.49 (2)	31.6 (5)	69.7 (6)	−133.0 (4)
TMSi#1	0.49 (2)	−126.9 (9)	39.7 (5)	119.0 (3)
TMSi#2	1.0	−67.3 (6)	138.0 (4)	−158.0 (9)
TMSi#3	1.0	133.7 (4)	114.9 (5)	−11.4 (9)
TMSi#4	0.51 (2)	31.6 (5)	69.7 (6)	−191.0 (3)
Second molecule				
TMC#5	0.51 (3)	−128.2 (6)	108.7 (5)	58.0 (3)
TMC#6	0.28 (2)	−22.4 (5)	69.4 (5)	161.0 (5)
TMC#7	0.21 (2)	63.1 (7)	132.3 (4)	119.0 (7)
TMSi#5	0.49 (3)	−128.2 (6)	108.7 (5)	106.0 (2)
TMSi#6	0.72 (2)	−22.4 (5)	69.4 (5)	115.0 (2)
TMSi#7	0.78 (2)	63.1 (7)	132.3 (4)	108.0 (2)
TMSi#8	1.0	126.7 (6)	42.7 (5)	68.1 (8)
Bu2				
First molecule				
TMC#1	0.53 (2)	−143.0 (1)	45.2 (9)	−117.0 (2)
TMC#2	1.0	−55.0 (7)	143.6 (4)	213.0 (9)
TMC#3	0.28 (2)	152.0 (2)	96.0 (1)	120.0 (3)
TMC#4	0.18 (2)	19.0 (3)	41.0 (3)	−25.0 (5)
TMSi#1	0.47 (2)	−125.0 (1)	37.4 (6)	−103.0 (2)
TMSi#3	0.72 (2)	134.8 (4)	96.0 (4)	117.7 (9)
TMSi#4	0.82 (2)	33.4 (4)	74.4 (4)	−41.0 (8)
Second molecule				
TMC#5	0.80 (2)	−138.1 (6)	114.8 (5)	−135.3 (8)
TMC#6	0.77 (1)	−29.2 (6)	56.2 (5)	26.0 (1)
TMC#7	0.43 (1)	66.7 (2)	143.0 (1)	8.0 (2)
TMSi#5	0.20 (2)	−125.0 (1)	97.0 (1)	−184.0 (3)
TMSi#6	0.23 (2)	−34.0 (1)	75.0 (1)	94.0 (3)
TMSi#7	0.57 (1)	68.0 (7)	122.4 (5)	−11.0 (1)
TMSi#8	1.0	121.0 (4)	45.3 (3)	66.5 (6)

The best fit converged at $R_p = 0.066$, $R_{wp} = 0.084$ and $R_{Bragg} = 0.048$ for 48 refined structural and 12 refined lattice, profile and background parameters (Fig. 6). Note that the R values are lower than in the initial model, while fewer independent parameters have been used.

A more accurate description of the disorder would require independent positions for the different orientations of the molecule at each site. Any attempt to extend the model in this way resulted in high correlations between parameters; a further improvement of the fit could not be obtained.

An equivalent description of the molecule with even fewer parameters is possible: the inner ($SiSi_3C$) core of the molecule has threefold symmetry with the Si—C bond as symmetry axis. Again, internal symmetry could be used to reduce the number of parameters. However, the construction of a quasi-rigid body from quasi-rigid bodies is not possible with the available software, and we did not pursue this type of model.

2.1.3. Refinement of Bu2 at 105 K. The low-temperature structure of Bu2 was analyzed in a similar way to the low-temperature structure of Bu1. A starting model was obtained with *DASH* and an initial structure refinement was performed with independent atoms and restraints. Subsequently, identical rotator groups were identified, and their orientations were defined analogously to those of Bu1 (Table 2). Occupancies and occupancy constraints were modified according to the different stoichiometry. Initially the constraints on the orientations of the rotator groups in the Bu1 refinement were applied to Bu2, but the resulting fit was of poorer quality than the refinement of Bu1 at the same stage. The quality of the refinement was considerably improved after eliminating those constraints that forced identical orientations of the $Si—Si(CH_3)_3$ and $Si—C(CH_3)_3$ groups. During the refinement, it became apparent that for both molecular sites the molecules are orientated such that one direction is completely occupied by one type of rotator group, $Si—C(CH_3)_3$ for the first and $Si—Si(CH_3)_3$ for the second site, while in the other three directions a mixture of both types of rotator groups is present. For both molecular sites, the $C—(CH_3)_3$ distribution favors two directions (Table 3). The best fit converged at $R_p = 0.067$, $R_{wp} = 0.089$, $R_{Bragg} = 0.043$ and included 62 structural parameters and 12 parameters for peak profile, background and lattice parameters (Fig. 7).

2.1.4. Refinement of the room-temperature structures. The room-temperature structures of both compounds have been found to have cubic lattices (Table 1). The starting point for the Rietveld refinements, which employed *JANA*2000, were again the profile and background functions as determined by the Le Bail fits (§2.1.1). Similarities with published high-temperature structures of other plastic crystals implied a c.c.p. structure with space group $Fm\bar{3}m$ and with a high degree of orientational disorder of the molecules (Dinnebier *et al.*, 1999, 2000, 2002).

The first structure model involved a set of spherical shells of electron density, which correspond to freely rotating molecules, in the case of dynamic disorder, or to randomly oriented molecules, in the case of static disorder. In this model, the scattering was described by the sum of the scattering of a

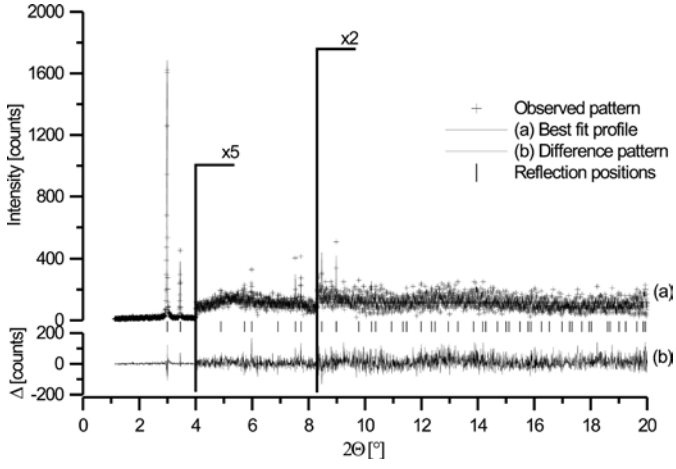

Figure 8
Best fit profile of the Rietveld refinement of Bu1 at room temperature using a model with spherical shells of electron density.

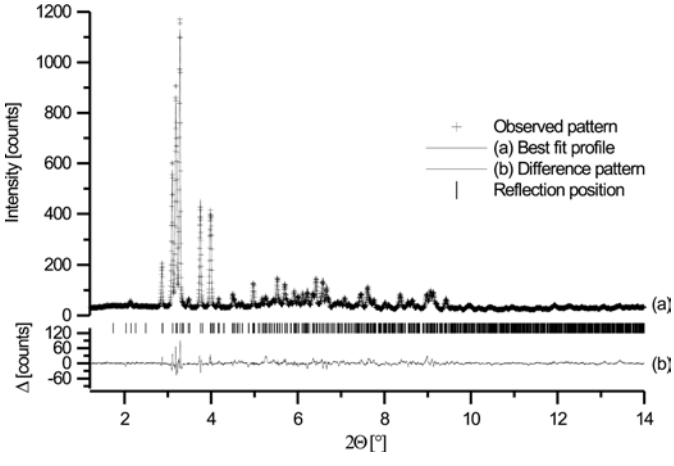

Figure 7
Best fit profile of the Rietveld refinement of Bu2 at 105 K with disordered rigid rotator groups.

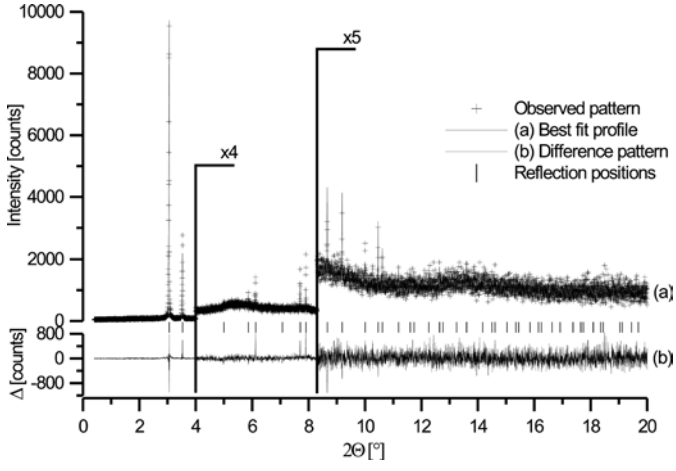

Figure 9
Best fit profile of the Rietveld refinement of Bu2 at room temperature using a model with spherical shells of electron density.

central Si atom, two spherical shells with the scattering power of the remaining Si or C atoms of the molecular core, and two spherical shells with the scattering power of the two types of methyl groups. The radii of the shells were obtained from the optimal molecular geometry as computed from the literature (*International Tables for Crystallography*, 1995, Vol. C). If refined, the radii became unstable and had implausible values, so the radii were kept fixed during the refinement. One overall isotropic temperature factor was refined. The Rietveld refinements converged at $R_p = 0.196$, $R_{wp} = 0.268$, $R_{Bragg} = 0.047$ for Bu1 and at $R_p = 0.148$, $R_{wp} = 0.209$, $R_{Bragg} = 0.223$ for Bu2.

Inspection of the experimental pattern showed that the (111) and (200) reflections are much stronger than the others and that the scattered intensity rapidly decreases with increasing scattering angle (Figs. 8 and 9). This behavior is characteristic of structures with a high degree of disorder. However, the decrease of intensity in the spherical-shell model was even greater than that in the experimental pattern. This observation indicates that the orientational disorder of the molecules is incomplete.

Therefore, further models were considered comprising molecules placed at the c.c.p. site in different orientations. The molecule was defined to have internal C_{3v} symmetry (Bu1) or C_{2v} symmetry (Bu2). The refinement of Bu1, where only a global isotropic temperature factor and the orientation of the molecule were refined, did not converge because the quality of the data was low. For Bu2 one overall isotropic temperature factor and the orientation of the molecule were varied in the refinement, while the internal geometry had to be kept fixed. The low quality of the data prevented refinement of additional parameters. The best fit was obtained for one molecule placed in a general orientation (Table 1). The high site symmetry then implies a 48-fold orientational disorder. Poorer fits were obtained for the molecule placed in special orientations that correspond to less than 48-fold disorder. It is thus concluded that the room-temperature structure of both compounds is c.c.p., with an orientational disorder of the molecules between 48-fold disorder and free rotation.

2.2. X-ray diffraction at high pressures

High-pressure X-ray powder diffraction experiments at room temperature were performed at station ID30 of the European Synchrotron Radiation Facility (ESRF). The samples were loaded into membrane-driven diamond anvil cells (DACs) (Letoullec *et al.*, 1988), which were equipped with 600 μm culet diamonds and stainless-steel gaskets with 250 μm-diameter holes. Silicon oil was used as the pressure medium. The pressure was determined by the ruby luminescence method using the wavelength shift calibration of Mao *et al.* (1986). X-rays of wavelength 0.3738 Å were selected with a (111) channel-cut Si monochromator, which was operated in a vacuum (water cooled) and irradiated by synchrotron radiation from two phased undulators of period 40 μm. The X-ray beam, with an initial size of 0.3 × 0.3 mm, was collimated down to a FWHM of 0.080 × 0.080 mm with tungsten carbide slits. Diffracted intensities were recorded with a Marresearch Mar345 online image-plate detector system. Series of 17 images were measured at 17 selected pressures between 0.05 and 4.79 GPa for Bu1, and at 17 selected pressures between 0.10 and 5.55 GPa for Bu2 . The exposure time of each image was 100 s. Data reduction was performed with the program *FIT2D* (Hammersley *et al.*, 1998), which produced diagrams of

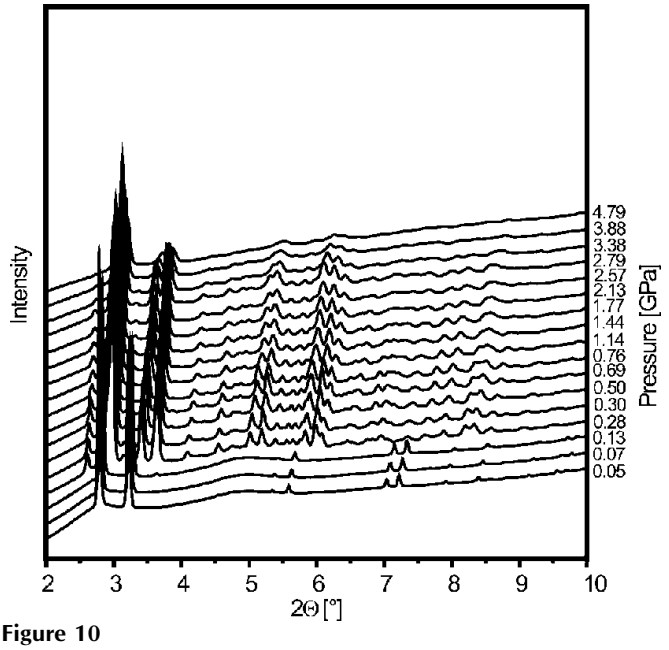

Figure 10
X-ray diffraction diagrams of the high-pressure experiments for Bu1. Note the high level of the background. A phase transition can be seen between 0.13 and 0.28 GPa. No additional phase transitions are obvious at higher pressures.

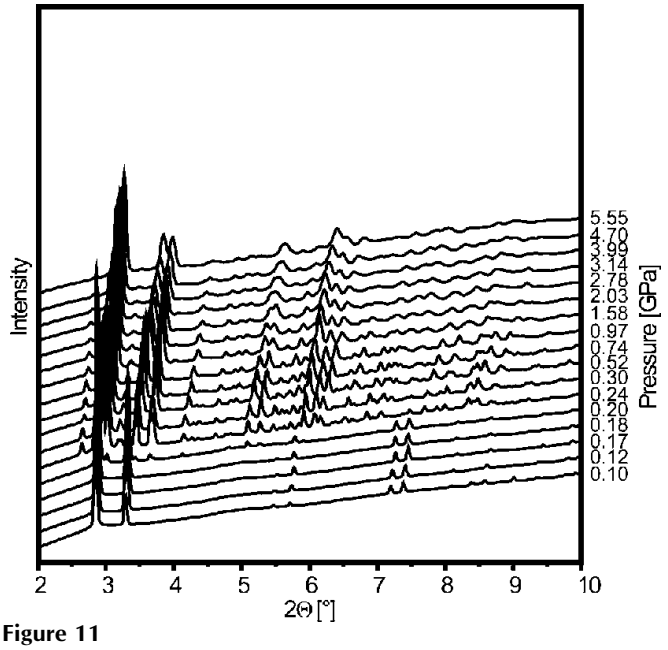

Figure 11
X-ray diffraction diagrams of the high-pressure experiments for Bu2. Note the high level of the background. A phase transition can be seen between 0.20 and 0.24 GPa. No additional phase transitions are obvious at higher pressures.

Table 4
Parameters of the Vinet equations of state for the different high-pressure phases of Bu1 and Bu2.

The fit parameters are V_0/Z, the volume per molecule at pressure 0 GPa, the bulk modulus K_0 and the pressure derivative of the bulk modulus K'.

	Pressure range	V_0/Z (Å^3)	K_0 (GPa)	K'
Bu1 cubic	0–0.2 GPa	603 (8)	1.3 (3)	4.0
Bu1 monoclinic	0.3–2.8 GPa	682 (17)	0.025 (1)	29.835
Bu1 monoclinic	2.8–4.8 GPa	520 (2)	20.9 (3)	0
Bu2 cubic	0–0.2 GPa	568 (4)	2.2 (3)	4.0
Bu2 monoclinic	0.2–1.6 GPa	539 (2)	2.47 (9)	12.27
Bu2 monoclinic	1.6–3.0 GPa	461 (1)	39 (1)	0
Bu2 monoclinic	3.0–5.5 GPa	467 (2)	33.6 (9)	0

corrected intensities *versus* scattering angle 2Θ (Figs. 10 and 11). Up to pressures of 0.13 GPa for Bu1 and 0.20 GPa for Bu2 the data could be indexed with *F*-centered cubic cells, while for pressures above 0.28 (Bu1) and 0.24 GPa (Bu2) monoclinic lattices, similar to the lattices of the low-temperature structures, were found. For all data sets, lattice parameters were obtained by Le Bail-type fits with the program *JANA*2000. The results are available as supplementary material. The slightly asymmetric peak profiles were described with a pseudo-Voigt peak-profile function and an empirical asymmetry correction. A manual background was used. From the analysis of the systematic absences, the space group $P2_1/n$ was established for the high-pressure structures.

The pressure dependence of the relative volumes of the unit cells was fitted with Vinet-type equations of state (Vinet *et al.*, 1986),

$$p = 3K_0(1 - f_V)f_V^{-2}\exp\left[3(K' - 1)(1 - f_V)/2\right], \qquad (1)$$

where $f_V = (V/V_0)^{1/3}$ and V is the volume for pressure p. The program *EOSFIT* (Angel, 2000) was used for these calculations and the results are given in Table 4.

3. Discussion

3.1. Low-temperature structures and phase transitions

$Si[C(CH_3)_3][Si(CH_3)_3]_3$ and $Si[C(CH_3)_3]_2[Si(CH_3)_3]_2$ are isostructural in their high-temperature phases. The molecules are arranged in a cubic close packing with a high degree of orientational disorder. Such a c.c.p.-type phase appears to be a common high-temperature phase of this class of plastic crystals (Dinnebier *et al.*, 1999, 2000, 2002).

Phase transitions towards monoclinic structures were found at $T_c = 230$ (5) K for Bu1 and at $T_c = 250$ (5) K for Bu2 (Figs. 3, 4, 12 and 13). Below the phase transition the molecules in the structure were still found to be disordered over two or three orientaions. The disorder can be described as the exchange of $C(CH_3)_3$ and $Si(CH_3)_3$ groups within the molecule. From our experiments it is not possible to determine whether the disorder is dynamic (reorientational jumps) or static.

The packing of the low-temperature structures can be described as a strongly distorted c.c.p. stacking (Figs. 14–17).

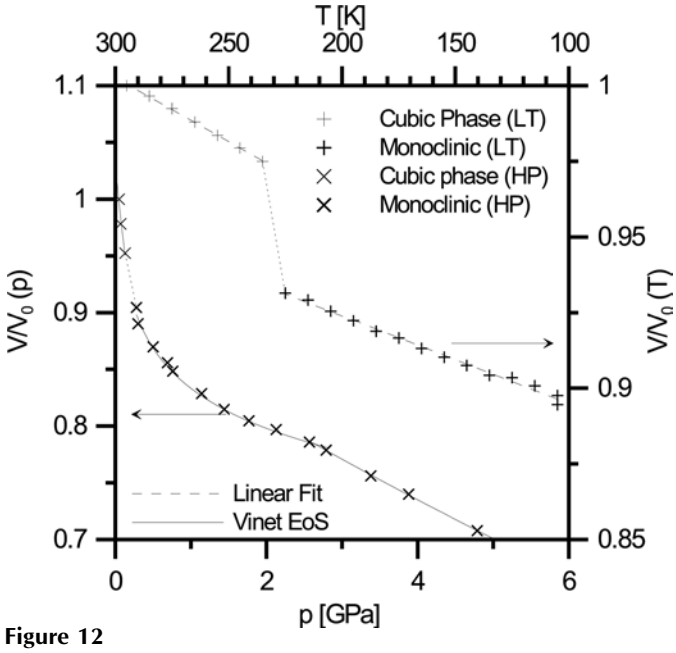

Figure 12
Temperature and pressure dependence of the molecular volume of Bu1. The cubic-to-monoclinic phase transition was observed between 235 and 225 K for the low-temperature experiment and between 0.13 and 0.28 GPa for the high-pressure experiment. The *p*–*V* curves have been fitted with Vinet equations of state (see text), the *T*–*V* curves with linear curves $V/V_0 = mT + v$ with $m = 0.00042$ K^{-1}, $v = 0.87601$ for the cubic phase and $m = 0.00029$ K^{-1}, $v = 0.86590$ for the monoclinic phase.

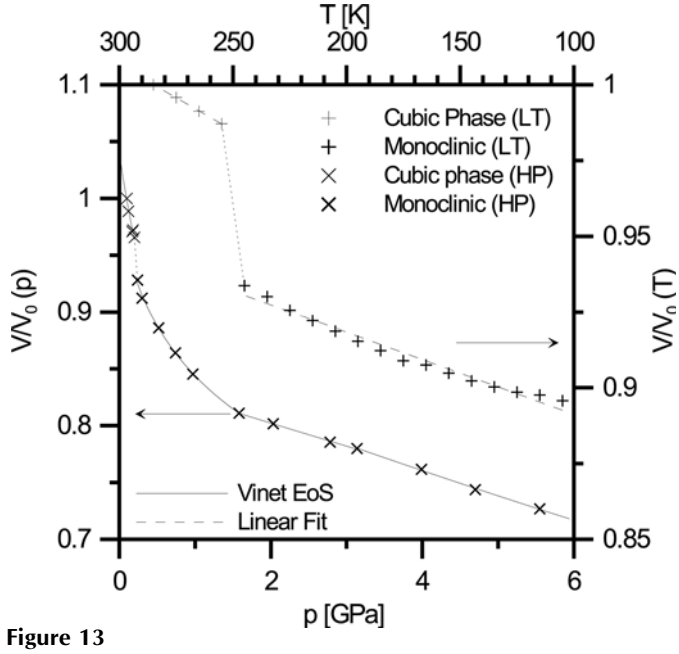

Figure 13
Temperature and pressure dependence of the molecular volume of Bu2. The cubic-to-monoclinic phase transition was observed between 235 and 225 K for the low-temperature experiment and between 0.20 and 0.24 GPa for the high-pressure experiment. The *p*–*V* curves have been fitted with Vinet equations of state (see text), the *T*–*V* curves with linear curves $V/V_0 = mT + v$ with $m = 0.00043$ K^{-1}, $v = 0.87725$ for the cubic phase and $m = 0.00027$ K^{-1}, $v = 0.86403$ for the monoclinic phase.

The monoclinic unit cells are related to the f.c.c. lattice by the transformation

$$\begin{pmatrix} \mathbf{a}' \\ \mathbf{b}' \\ \mathbf{c}' \end{pmatrix} = \begin{pmatrix} 1 & 1 & 0 \\ -1 & 1/2 & -1/2 \\ -1/2 & 1/2 & 1 \end{pmatrix} \begin{pmatrix} \mathbf{a} \\ \mathbf{b} \\ \mathbf{c} \end{pmatrix}. \qquad (2)$$

The transformation (2) results in a triclinic cell from which the monoclinic cell is obtained by a small distortion (Fig. 18).

In the monoclinic structures the (010) plane can be identified as an approximately close-packed plane. It corresponds to the $(1\bar{1}1)$ plane of the cubic cell (2). Within the $(010)_m$ plane the molecules have six neighbors arranged in a distorted hexagon. In a c.c.p. structure there should be three nearest neighbors above and below the close-packed plane. However, in the monoclinic structure we find up to four neighbors above and below the $(010)_m$ plane, with a wide range of distances (Figs. 19 and 20). Thus, the first coordination sphere contains 14 molecules instead of 12 in the case of a c.c.p. structure. The distances of these 14 molecules to the central molecule vary between 8.219 and 11.531 Å for Bu2 and 8.527 and 11.672 Å for Bu1.

These distances are determined by two factors: the orientation of the core tetrahedron of one molecule in the contact to the core tetrahedron of the other molecule, and the fraction of $Si-C(CH_3)_3$ groups in the contact. A core tetrahedron shows one of the three basic orientations with respect to the connection line between the centers of two molecules. These basic types are hereafter called 'face', 'edge' and 'vertex' (Fig. 21) and can best be classified by the values of the angles Si(0)(molecule1)—Si(1)/C(1)(molecule1)—Si(0)(molecule2)

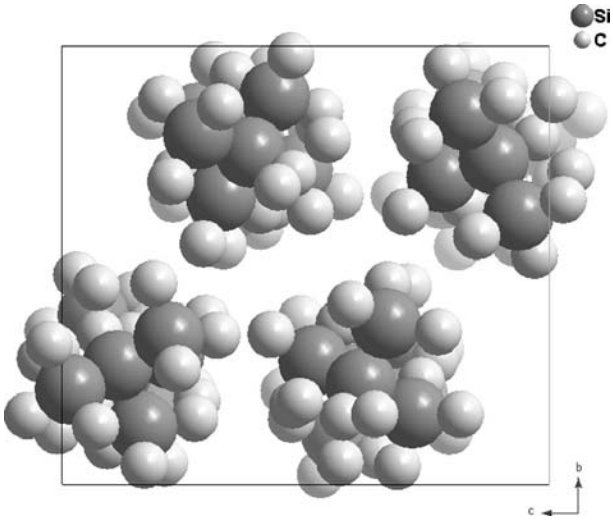

Figure 14
Structure of the low-temperature phase of Bu1 viewed along **x**. For clarity the most probable orientations of the disordered molecules are used. The content of one unit cell is displayed.

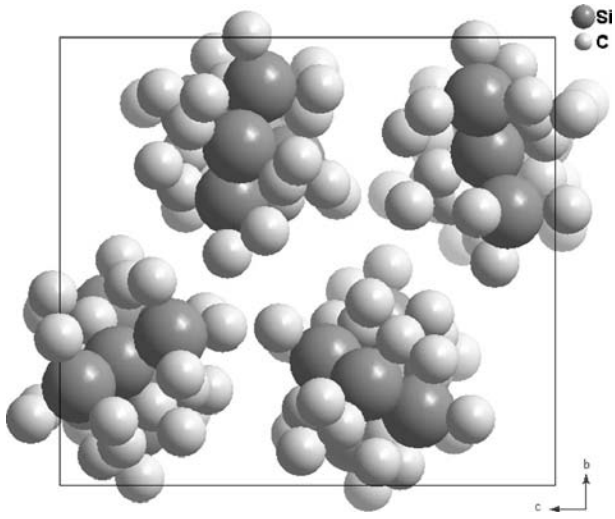

Figure 16
Structure of the low-temperature phase of Bu2 viewed along **x**. For clarity the most probable orientations of the disordered molecules are used. The content of one unit cell is displayed.

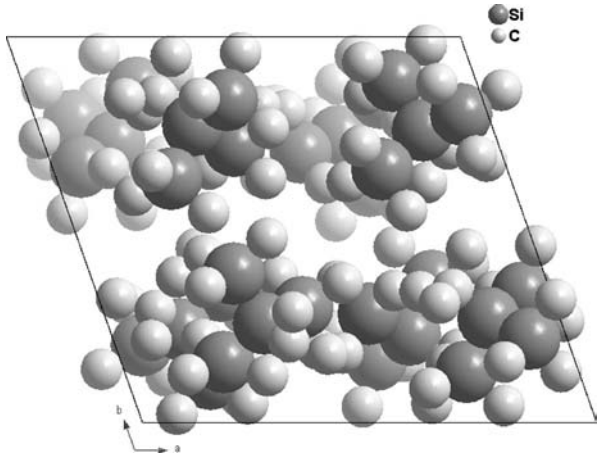

Figure 15
Structure of the low-temperature phase of Bu1 viewed along **z**. For clarity the most probable orientations of the disordered molecules are used. The content of one unit cell is displayed.

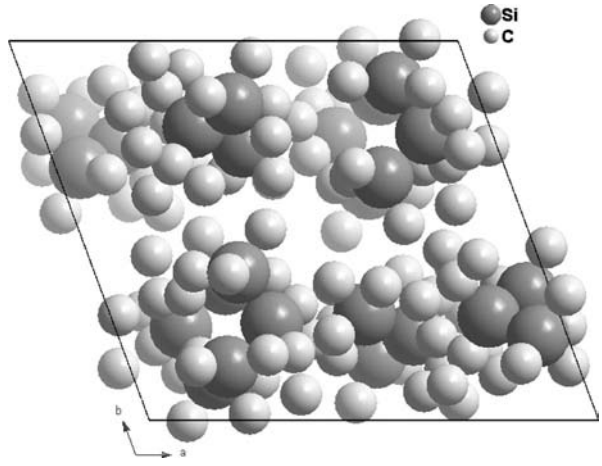

Figure 17
Structure of the low-temperature phase of Bu2 viewed along **z**. For clarity the most probable orientations of the disordered molecules are used. The content of one unit cell is displayed.

Table 5
Dependence of the distances d of the centers of two molecules on the contact type (see text) and the fraction C of $C(CH_3)_3$ groups in the contacts.

Bu1			Bu2		
d (Å)	Type of contact	C (%)	d (Å)	Type of contact	C (%)
8.527	face–face	33.3	8.219	edge–edge	77.5
8.563	edge–edge	32.3	8.290	face–edge	52.2
8.638	edge–edge	25.0	8.599	face–face	57.0
8.759	edge–edge	17.7	8.648	edge–edge	50.3
8.798	face–edge	20.0	8.680	edge–face	45.6
8.798	edge–face	20.0	8.680	face–edge	45.6
8.801	face–edge	20.2	8.808	edge–edge	22.5
9.185	edge–face	16.5	8.898	edge–face	47.6
9.708	vertex–vertex	49.9	9.362	vertex–vertex	71.5
9.907	vertex–vertex	25.4	9.791	vertex–vertex	49.0
9.912	vertex–vertex	10.8	9.861	vertex–vertex	26.5
10.528	edge–vertex	16.4	9.929	vertex–vertex	64.0
10.528	vertex–edge	16.4	9.929	vertex–vertex	64.0
11.672	vertex–vertex	50.7	11.531	vertex–vertex	53.0

of all rotator groups of molecule 1. In the ideal case, three of these angles are 70.53° and one is 180° for a face; two angles are 54.75° and the other two angles are 125.25° for an edge; and one angle is 0° and three angles are 109.47° for a vertex. None of the observed contacts was equal to one of these ideal cases, but for most of the observed contacts a classification into one of the three types was straightforward. A few contacts were difficult to classify, so the sums of the squares of the difference angles between the ideal and observed contact were calculated for all contact types and the minimum was chosen.

The distances found for the 14 neighbors for both compounds along with a classification of the contact type and the content of $Si-C(CH_3)_3$ in the contact are given in Table 5. For contacts where faces and edges are involved, shorter distances are found, while contacts with vertices are systematically longer. These results can be understood if we consider the geometrical aspects of the packing. Edge- and face-type contacts allow the groups of different molecules to avoid each other. In a projection along the contact, the edges prefer to be perpendicular in the gaps between the other edge. For faces the preferred arrangement is two triangles where the second is rotated by an angle of π with respect to the first (Fig. 21). The amount of $Si-C(CH_3)_3$ fragments seems to have a minor influence, but the correlation can be seen for contacts of the same basic type. Shorter contacts require smaller molecules and thus a larger fraction of the molecules are oriented with an $Si-C(CH_3)_3$ group in this direction.

In this class of plastic crystals, only short-range interactions between the non-polar molecules are present. The weak van der Waals attractions and especially the Born repulsion and

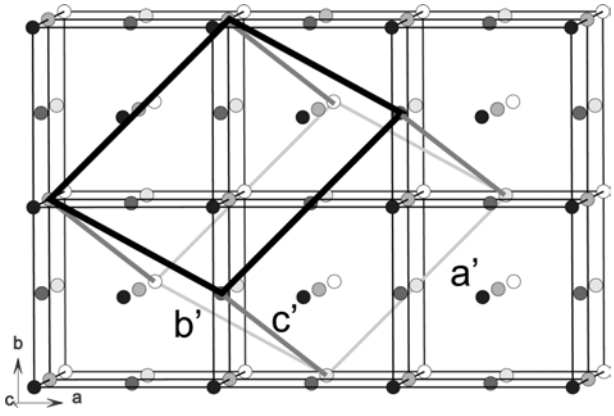

Figure 18
Relation between the monoclinic unit cell of the low-temperature phase and the cubic unit cell at room temperature using the transformation of (2).

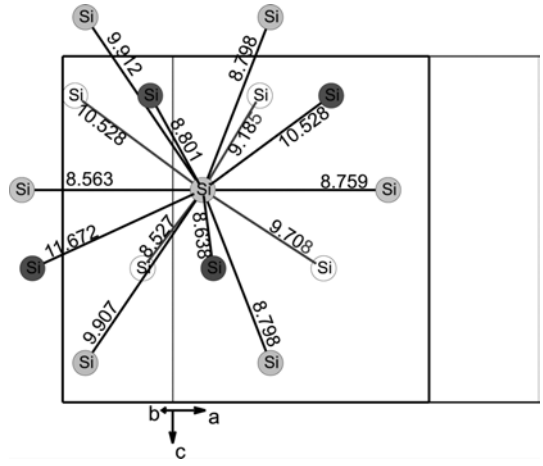

Figure 19
Packing of the Bu1 molecules in the low-temperature phase. The distances between the centers of the molecules are given. For clarity only the central Si atoms of the molecules are shown. The molecules are arranged in three planes perpendicular to the view along **b***. The darkness of the atoms indicates the distance from the viewer (dark = close).

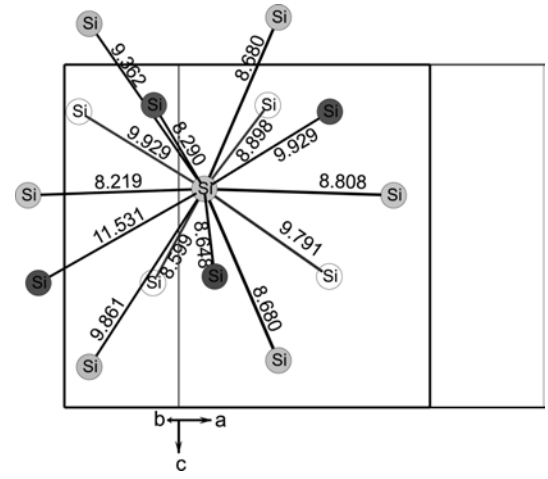

Figure 20
Packing of the Bu2 molecules in the low-temperature phase. The distances between the centers of the molecules are given. For clarity only the central Si atoms of the molecules are shown. The molecules are arranged in three planes perpendicular to the view along **b***. The darkness of the atoms indicates the distance from the viewer (dark = close).

consequently the different shapes of the molecules determine the packing. The shape of the smaller molecules $C[Si(CH_3)_3]_4$ and $Si[Si(CH_3)_3]_4$ is in closest agreement with a sphere and the packing is in closest agreement with the packing of spheres, since the centers of the molecules are at positions corresponding to a c.c.p. arrangement (Dinnebier *et al.*, 1999). The larger molecules $Si[Sn(CH_3)_3]_4$ and $Ge[Sn(CH_3)_3]_4$ have large gaps between the $Sn(CH_3)_3$ groups and so their shape deviates from a perfect sphere, as does their packing, which corresponds to a distorted c.c.p. structure (Dinnebier *et al.*, 2002). The Bu1 and Bu2 molecules are small, as are the gaps between the rotators. However, the intrinsic asphericity of these molecules results in a distorted c.c.p. arrangement, which is of a different kind from that of $Si[Sn(CH_3)_3]_4$ and $Ge[Sn(CH_3)_3]_4$.

3.2. High-pressure behavior

Phase transitions from c.c.p. structures towards monoclinic structures were found at pressures of 0.13–0.28 GPa for Bu1 and at pressures of 0.20–0.24 GPa for Bu2. The high-pressure phases have similar lattice parameters to the low-temperature structures and the same space group $P2_1/n$ as the low-temperature structures. Therefore we conclude that the high-pressure structures are isostructural to the low-temperature structures. Further support for this interpretation is given by the similar distributions of peak intensities in the low-temperature and high-pressure powder diffraction patterns (Figs. 3, 10, 4 and 11). However, structure refinements of the high-pressure structures that used the structure model of the low-temperature structures did not succeed because of the significantly lower quality of the data.

A singularity of the slope can be seen in the p–V curve of Bu1 at a pressure of 2.8 GPa (Fig. 12). Similar behavior is found for Bu2 at 1.6 GPa and 3.0 GPa (Fig. 13). While the pressure dependencies of the lattice parameters are relatively homogeneous throughout the observed pressure range, at the pressures of these anomalies and at slightly higher pressures the lattice parameters behave inhomogeneously. There is a large decrease in one of the lattice parameters and a small increase in another. Thus one direction appears to become softer while the others keep or even slightly increase their rigidity.

The anomalies can be explained with additional ordering phase transitions. In the low-temperature structures at 105 K, orientational disorder of the molecules over two or three orientations is present. This disorder is also assumed to be present in the isostructural high-pressure phase. At the transitions, these additional orientations are lost. The lattice shrinks in directions where $Si-C(CH_3)_3$ groups lock in, while the lattice expands in directions where $Si-Si(CH_3)_3$ groups lock in.

The bulk moduli of Bu1 and Bu2 indicate that at lower pressures these materials are even softer than $C[Si(CH_3)_3]_4$ ($K_0 = 7.1$ GPa) (Dinnebier *et al.*, 2000) or $Si[Si(CH_3)_3]_4$ ($K_0 = 3.7$ GPa) (Wunschel *et al.*, 2003). This result can be explained by the different shapes of the molecules and the better filling of space of the more spherical molecules of the latter two compounds.

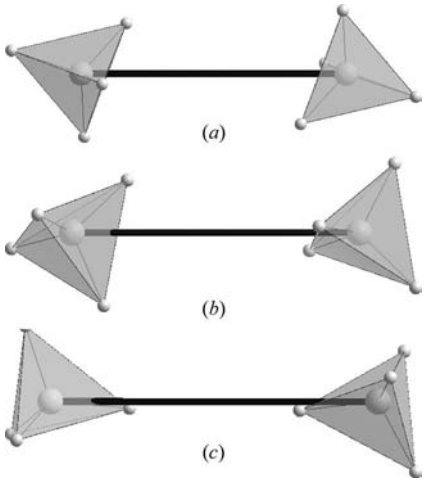

Figure 21
Typical representatives of the three basic contact types, face–face (*a*), edge–edge (*b*) and vertex–vertex (*c*), of the Bu1 and Bu2 molecules. Note the tendency of the face–face and edge–edge contacts to orient the faces/edges to avoid the face/edge of the other molecule.

4. Conclusions

The room- and low-temperature crystal structures of $Si[C(CH_3)_3]_1[Si(CH_3)_3]_3$ (Bu1) and $Si[C(CH_3)_3]_2[Si(CH_3)_3]_2$ (Bu2) have been determined by X-ray powder diffraction and Rietveld refinements. At room temperature both compounds form a c.c.p. structure with a high degree of orientational disorder of the molecules. Below $T_c = 230$ (5) K (for Bu1) and $T_c = 250$ (5) K (for Bu2) the crystal structures are monoclinic and correspond to a highly distorted c.c.p. A detailed analysis of the structural data showed that the symmetries and packings at low temperatures can be understood from optimized packing of the molecules. Depending on the shapes of the molecules, symmetries $P2_13$ $\{C[Si(CH_3)_3]_4$ and $Si[Si(CH_3)_3]_4\}$, $P2_1/n$ (Bu1 and Bu2) and $P\bar{1}$ $\{Si[Sn(CH_3)_3]_4$ and $Ge[Sn(CH_3)_3]_4\}$ are thus obtained.

The room-temperature structures transform to monoclinic phases at pressures of 0.13–0.28 GPa (Bu1) and 0.20–0.24 GPa (Bu2). These high-pressure phases are probably isostructural to the low-temperature phases. At still higher pressures, anomalies in the pressure dependence of the volume of the unit cell indicate further phase transitions. They might correspond to a removal of the remaining disorder that was established for the monoclinic phases at low temperatures.

Measurements have been carried out at the European Synchrotron Radiation Facility (ESRF) at beamlines ID30 and BM16. We thank Andy Fitch for his support during the measurements. Financial support by the Deutsche Forschungsgemeinschaft (DFG) (Project Di687-4), the VCI and the BMBF is gratefully acknowledged.

References

Angel, R. J. (2000). *VII Workshop Powder Diffraction – Structure Determination and Refinement from Powder Diffraction Data*, edited by R. E. Dinnebier. Ber. aus den Arbeitskreisen der DGK 9. Deutsche Gesellschaft für Kristallographie.

Becker, G., Hartmann, H.-M., Münch, A. & Riffel, H. (1985). *Z. Anorg. Allg. Chem.* **530**, 29–42.

David, W. I. F. & Shankland, K. (2001). *DASH. Program for Structure Solution from Powder Diffraction Data.* Cambridge Crystallographic Data Centre, Cambridge, England.

David, W. I. F., Shankland, K. & Shankland, N. (1998). *Chem. Commun.* pp. 931–932.

Dinnebier, R. E., Bernatowicz, P., Helluy, X., Sebald, A., Wunschel, M., Fitch, A. & van Smaalen, S. (2002). *Acta Cryst.* B**58**, 52–61.

Dinnebier, R. E., Carlson, S. & van Smaalen, S. (2000). *Acta Cryst.* B**56**, 310–316.

Dinnebier, R. E., Dollase, W. A., Helluy, X., Kümmerlein, J., Sebald, A., Schmidt, M. U., Pagola, S., Stephens, P. W. & van Smaalen, S. (1999). *Acta Cryst.* B**55**, 1014–1029.

Dinnebier, R. E. & Finger, L. (1998). *Z. Kristogr. Suppl.* **15**, 148.

Dušek, M., Petříček, V., Wunschel, M., Dinnebier, R. E. & van Smaalen, S. (2001). *J. Appl. Cryst.* **34**, 398–404.

Finger, L. W., Cox, D. E. & Jephcoat, A. P. (1994). *J. Appl. Cryst.* **27**, 892–900.

Fitch, A. N. (1996). *Mater. Sci. Forum*, **228–231**, 219–222.

Fujiki, S., Kubozono, Y., Kobayashi, M., Kambe, T., Rikiishi, Y., Kashino, S., Ishii, K., Suematsu, H. & Fujiwara, A. (2002). *Phys. Rev. B*, **65**, 235425–1–235425–7.

Hammersley, A. P., Svensson, S. O., Hanfland, M., Fitch, A. N. & Hausermann, D. (1998). *High Press. Res.* **14**, 235–248.

Helluy, X., Kümmerlen, J. & Sebald, A. (1998). *Organometallics*, **17**, 5003–5008.

Hodeau, J. L., Bordet, P., Anne, M., Prat, A., Fitch, A. N., Dooryhee, E., Vaughan, G. & Freund, A. (1998). *Proc. SPIE*, **3448**, 353–361.

Kohlbeck, F. & Hörl, E. M. (1976). *J. Appl. Cryst.* **9**, 28–33.

Kohlbeck, F. & Hörl, E. M. (1978). *J. Appl. Cryst.* **11**, 60–61.

Larson, A. C. & von Dreele, R. B. (1994). *GSAS.* Los Alamos National Laboratory Report LAUR 86–748, Los Alamos National Laboratory.

Le Bail, A., Duroy, H. & Fourquet, J. L. (1988). *Mater. Res. Bull.* **23**, 447–452.

Letoullec, R., Pinceaux, J. P. & Loubeyre, P. (1988). *High Press. Res.* **1**, 77–90.

Mao, H. K., Xu, J. & Bell, P. M. (1986). *J. Geophys. Res.* **91**, 4673–4676.

Nakayama, A., Fujihisa, H., Aoki, K. & Carlon, R. P. (2000). *Phys. Rev. B*, **62**, 8759–8765.

Nowell, H., Attfield, P., Cole, J. C., Cox, P. J., Shankland, K., Maginn, S. J. & Motherwell, W. D. S. (2002). *New J. Chem.* **26**, 469–472.

Petříček, V. & Dušek, M. (2000). *The crystallographic computing system JANA*2000. Institute of Physics, Academy of Sciences of the Czech Republic, Praha, Czech Republic.

Shirley, R. (2000). *The CRYSFIRE System for Automatic Powder Indexing: User's Manual.* Guildford, Surrey, UK: The Lattice Press.

Smrcok, L., Koppelhuber-Bitschnau, B., Shankland, K., David, W. I. F., Tunega, D. & Resel, R. (2001). *Z. Kristallogr.* **216**, 63–66.

Thompson, P., Cox, D. E. & Hastings, J. B. (1987). *J. Appl. Cryst.* **20**, 79–83.

Vinet, P., Ferrante, J., Smith, J. R. & Rose, J. H. (1986). *J. Phys. C*, **19**, L467–L473.

Wunschel, M., Dinnebier, R. E., Carlson, S. & van Smaalen, S. (2003). Submitted.